Inorganic Chemistry

Communication

pubs.acs.org/IC

Distinct Packings of Supramolecular Building Blocks in Metal–Organic Frameworks Based on Imidazoledicarboxylic Acid

Qingqing Pang,[†] Binbin Tu,[†] Erlong Ning,[†] Qiaowei Li,*[,†,§] and Dongyuan Zhao[†,‡,§]

[†]Department of Chemistry, [‡]Laboratory of Advanced Materials, and [§]iChEM (Collaborative Innovation Center of Chemistry for Energy Materials), Fudan University, Shanghai 200433, P. R. China

Supporting Information

ABSTRACT: When the supramolecular building block packings (face-centered, body-centered, and primitive cubic) with different interactions (hydrogen and coordination bonding) were controlled, four new structures based on octahedral M^{II} (M = Zn, Ni, Mn) and imidazoledicarboxylate were constructed. The interaction modes between the supramolecular building blocks affect the water stability of the structures. Furthermore, with uncoordinated carboxylate O atoms in the structures, these compounds demonstrate a strong capability of capturing metal ions in the solution.

Inorganic secondary building units[1] in metal–organic frameworks (MOFs)[2] are usually metal ions or molecular clusters. Metal–organic polyhedra,[3] with sites that could further coordinate to neighboring entities, can serve as supramolecular building blocks (SBBs)[4] for complex framework construction. These SBBs usually have more coordination sites than simple metal ions or clusters, acting as nodes with high connectivity and symmetry. For example, 4,5-imidazoledicarboxylic acid (H_3ImDC; Figure 1a) tends to assemble with six-coordinated metal ions to form cubes (Figure 1b), functioning as SBBs with up to 24 carboxylate O atoms on the surfaces.[5] These peripheral O atoms provide potential hydrogen-bonding sites with other cubes[5a−c] or coordination sites with extra metal ions[5d−i] to generate extended network structures. Two types of pores with distinct geometries and periodic arrangements can be achieved in these structures: the intrinsic cavities within the SBBs and the pores formed by linking these SBBs together.

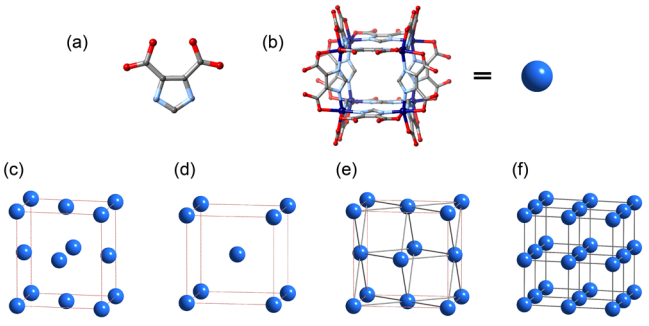

Figure 1. (a) H_3ImDC linker. (b) Cubic SBBs assembled by H_3ImDC linkers and metal ions. Schematic representation of packing modes for (c) FDM-11, (d) FDM-12, (e) FDM-13, and (f) FDM-14. The gray bonds indicate that these SBBs are connected by coordination bonds. The red dotted lines are shown to highlight the packings of SBBs.

To demonstrate this strategy in obtaining extended structures with different arrangements of the same cubic SBBs systematically and to further investigate how the arrangements contribute to the openness of the frameworks, we report four new structures from octahedral M^{II} (M = Zn, Ni, Mn) and H_3ImDC. Discrete face-centered-cubic (fcc) packing of SBBs by hydrogen bonding (for FDM-11, Figure 1c), discrete body-centered-cubic (bcc) packing of SBBs with compensating complex ions fixed between (for FDM-12, Figure 1d), fcc packing (for FDM-13, Figure 1e), and primitive-cubic (pcu) packing (for FDM-14, Figure 1f) of SBBs with extra M^{II} connecting them were observed. With almost identical SBB cavity sizes for all four structures, their characteristic packing modes have shaped distinct pores in the structures. FDM-13, in which the SBBs are connected with coordination bonds, shows high structural stability in water. In addition, the uncoordinated O atoms in FDM-11, -12, and -13 are capable of capturing metal ions in the solution, suggesting the activities of these sites for further application in heavy-metal removal.

FDM-11 ($[Zn_8(HImDC)_{12}\cdot(Me_2NH_2)_8\cdot(EtOH)]$) was synthesized by the reaction of $Zn(NO_3)_2\cdot 6H_2O$ with H_3ImDC in an *N*,*N*-dimethylformamide (DMF)/ethanol mixture at 100 °C. The structure of FDM-11 was determined by single-crystal X-ray diffraction (Table S1 in the Supporting Information, SI) and found to be a molecular packing of Zn-based metal–organic cubes (Figure 2a). Interestingly, the cubes are packed in a discrete fcc mode with intermolecular hydrogen-bonding interactions between the adjacent cubes (the closest O–H···O distance of 3.09 Å; Figure 2b). This structure is analogous to a previously reported Ni-based cube,[5g] and the largest sphere that can fit into the inner cavity of the cube without touching the van der Waals surface has a diameter of 4.4 Å.

When Ni^{II} was employed as the metal in a different reaction condition, FDM-12 ($\{Ni_8(HImDC)_{12}\cdot[Ni(en)_3]_4\cdot(DMA)_2(H_2O)_4\}$, where en = ethylenediamine and DMA = *N*,*N*-dimethylacetamide) was obtained (see the SI). FDM-12 crystallizes in the cubic system with the $Im\bar{3}$ space group (Table S2 in the SI). The cubes are isostructural with those in FDM-11, with the Ni···Ni distance of 6.28 Å, serving as the SBBs for the structure. However, instead of hydrogen bonding between adjacent cubes, these SBBs are separated by $[Ni(en)_3]^{2+}$ complex ions, with an inter-SBB distance of 20.95 Å, as measured by the

Received: July 23, 2015
Published: September 30, 2015

DOI: 10.1021/acs.inorgchem.5b01659
Inorg. Chem. 2015, 54, 9678−9680

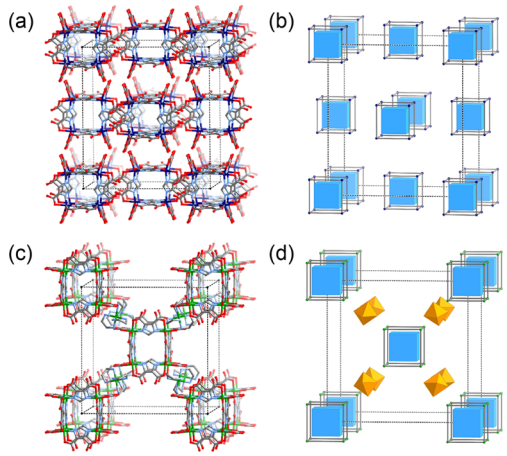

Figure 2. (a) Single-crystal structure and (b) schematic representation of FDM-11. (c) Single-crystal structure and (d) schematic representation of FDM-12.

distances between the body centers of the cubes (Figure 2c). Eight complex ions are located around each cube, making the cubes in FDM-12 pack in the bcc form (Figure 2d).

With the absence of ethylenediamine in the solution, a new MOF structure based on the same SBB was obtained. In FDM-13 ($[Ni_{12}(HImDC)_4(ImDC)_8(DMF)_4{\cdot}(H_3O)_8]$; Table S3 in the SI), the carboxylate O atoms from eight triply deprotonated linkers in each cube are concurrently connected to eight extra Ni^{II} ions in the octahedral geometry (Figure 3a). These bridges

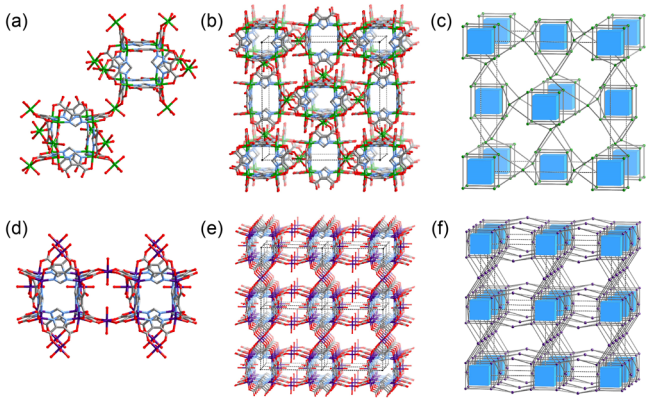

Figure 3. (a) Coordination of Ni^{II} between two adjacent SBBs in FDM-13. (b) Single-crystal structure and (c) schematic representation of FDM-13. (d) Coordination of Mn^{II} between two adjacent SBBs in FDM-14. (e) Single-crystal structure and (f) schematic representation of FDM-14.

connect the SBBs into an extended network structure (Figure 3b), where the SBBs are arranged in a fcc packing mode (Figure 3c). In FDM-13, the octahedron surrounded by six cubes has a cavity of ~10.6 Å diameter.

FDM-14 ($[Mn_{14}(ImDC)_{12}{\cdot}(H_3O)_8{\cdot}(DMA)_6(H_2O)_{10}]$; Table S4 in the SI), which is assembled from ideal Mn-based cubes with a Mn···Mn distance of 6.58 Å, shows a completely new structure by connecting these cubes in a different manner. Specifically, each cube is simultaneously connected through all of its 12 edges to 12 Mn^{II} ions, and two Mn^{II} form a pair to connect two neighboring cubes (Figures 3d,e). The cubes in FDM-14 are arranged in a pcu packing mode (Figure 3f).

With the same SBB size, they show various inter-SBB distances due to different interactions, as listed in Table 1. The SBBs in

Table 1. Structural Aspects of the Structures Studied

	a (Å)[a]	packing	d (Å)[b]	V (Å^3)[c]
FDM-11	6.28	fcc	16.94	3727
FDM-12	6.28	bcc	20.95	7078
FDM-13	6.30	fcc	17.92	4153
FDM-14	6.58	pcu	16.85	4741

[a]The cube edge distance (a) is the average value of the distances between the metal vertices along the cube edges. [b]The inter-SBB distance (d) is the average value of the centroid−centroid separations of neighboring cubes. [c]Volume per cube.

FDM-11 are assembled by hydrogen bonding, with an average centroid−centroid separation of neighboring cubes of 16.94 Å. FDM-13 and -14, whose SBBs are connected by additional metal ions, show similar inter-SBB distances (17.92 and 16.85 Å, respectively). Moreover, FDM-12 shows a much longer inter-SBB distance of 20.95 Å because of the insertion of complex ions between the cubes.

From solid materials packing theory, we know that the sphere packing modes of the solids determine the filled space and the pore proportions of the material. Each cube in FDM-11 and -13 occupies 3727 and 4153 Å^3 in volume, respectively, as calculated by the cell volume divided by the number of cubes in each unit cell. The same cube in FDM-14 occupies 4741 Å^3, indicating that, with pcu packing of SBBs, FDM-14 has created more empty spaces around the SBBs compared to FDM-11 and -13. This is in line with the observation that fcc packing has a lower pore percentage compared to pcu packing in classical sphere packing. On the other hand, even though FDM-12 has bcc packing of SBBs, which usually corresponds to a lower free-volume percentage than pcu packing in the cell, it has the largest volume per cube in our investigation (7078 Å^3). This can be explained by the longest inter-SBB distance due to complex ion insertion. In addition to the sphere packing modes, the insertion of extra entities to modulate the distances between spheres has introduced a new way to further control the openness of these frameworks.

Analysis of the packing modes of solid materials has intrigued us to compare the calculated porosities of these structures. By preliminary modeling with *Materials Studio* software, FDM-11 and -12 show calculated Brunauer−Emmett−Teller (BET) surface areas of 526 and 2215 m^2 g^{-1}, respectively. This is the same trend as those with the packing modes (fcc with less free space vs bcc with more free space) and the inter-SBB distances (16.94 vs 20.95 Å). Sharing the same packing mode and similar inter-SBB distances with FDM-11, FDM-13 has a BET surface area of 732 m^2 g^{-1}. FDM-14 with pcu packing has a larger surface area (1544 m^2 g^{-1}) than FDM-11 and -13 with fcc packing. However, in accordance with several related studies on similar MOF structures,[5c,6] the N_2 isotherms of the activated samples at 77 K and the Ar isotherms at 87 K show almost no surface area, which could be due to possible framework collapse during activation (Figure S10 in the SI). However, this strategy clearly indicates that control over the assembly of one simple SBB could contribute to diverse structures with varied openness.

The bulk purities of the structures were confirmed by comparing the experimental to the simulated powder X-ray diffraction (PXRD) patterns (Figures S1−S4 in the SI). Thermogravimetric analysis further demonstrates their thermal

DOI: 10.1021/acs.inorgchem.5b01659
Inorg. Chem. 2015, 54, 9678−9680

stabilities (Figure S11 in the SI). FDM-14, which has more edge connection among neighboring SBBs and is therefore more rigid, shows much higher thermal stability up to 400 °C than others.

To further investigate how the different interaction modes between SBBs affect the chemical stabilities of the structures, the samples (~40 mg) were immersed in deionized water (8 mL) for 14 days at ambient temperature. After treatment with water, crystals of FDM-11 and -12 changed into amorphous powders immediately with no peak in the PXRD patterns, indicating that water molecules broke the weak hydrogen bonding between the SBBs. However, FDM-13 maintained its full crystallinity in water for 14 days (Figure S5 in the SI), while for FDM-14 (Figure S6 in the SI), the intensities of strong peaks in PXRD decreased along the time frame and the structural integrity was not retained after 9 days. A total of 1.3% of MOF crystals got decomposed in 5 days, as calculated by the free ligand concentration in water via UV−vis spectroscopy (Figure S12 in the SI).

On the surface of each cube in FDM-11, -12, and -13, there are 24, 24, and 8 uncoordinated O atoms, respectively, which could further coordinate to incoming metal ions. To demonstrate the capability of capturing extra metal ions in these positions,[7] the fresh samples were immersed in the solution of Cd^{II} with heating for 2 days (see the SI). As determined by inductively coupled plasma atomic emission spectrometry, the solids of FDM-11, -12, and -13 can uptake 8.1, 27.5, and 3.9 wt % Cd^{II} based on the final weight, respectively. FDM-13 maintained single crystallinity after Cd^{II} capture with the strongest peaks retained in PXRD (Figure S9 in the SI), and the uptake corresponds to 1.2 Cd^{II} per cube. On the other hand, FDM-11 and -12 have partially lost their crystallinity during the metal capture experiments (Figures S7 and S8 in the SI). FDM-11 and -12 were further used to test their Co^{II} and Cr^{III} capture capability, and the uptake values are listed in Table S5 in the SI. These studies clearly show that, with uncoordinated O atoms in the SBBs, FDM-11, -12, and -13 could further coordinate with extra metal ions, and the openness of the structures guarantees that metal-ion capture happens not only on the crystal surface but also in the pores of the structures.

In summary, we have successfully synthesized four structures based on cubic SBBs. FDM-11 and -12 are constructed by the fcc and bcc packing of SBBs with weak interactions. On the other hand, SBBs in FDM-13 and -14 are arranged in fcc and pcu packing modes, respectively, with extra metal coordinations. Resembling the simple sphere packing in solid structures, the pore proportions in the structures could be modulated by the inter-SBB distances and the distinct packing modes. FDM-13 exhibits high stability in water, which can be explained by the edge connections among the SBBs through the coordination bonds. The presented strategy in regulating the arrangements of building units will introduce new structures with precisely controlled porosities. Furthermore, the uncoordinated O atoms in structures have provided coordination sites for incoming heavy-metal ions, pointing to further application in capturing metal ions with high efficiency.

■ ASSOCIATED CONTENT

Supporting Information

The Supporting Information is available free of charge on the ACS Publications website at DOI: 10.1021/acs.inorgchem.5b01659.

Synthesis and characterization details (PDF)

CCDC 1414687−1414690 (CIF)

■ AUTHOR INFORMATION

Corresponding Author

*E-mail: qwli@fudan.edu.cn.

Notes

The authors declare no competing financial interest.

■ ACKNOWLEDGMENTS

This work was supported by the Shanghai Municipal Education Commission (14ZZ005), the Shanghai Rising-Star Program (15QA1400400), and the Science & Technology Commission of Shanghai Municipality (14JC1400700). We thank Prof. Linhong Weng for discussion in X-ray crystallography.

■ REFERENCES

(1) O'Keeffe, M.; Yaghi, O. M. *Chem. Rev.* **2012**, *112*, 675−702.

(2) (a) Yaghi, O. M.; O'Keeffe, M.; Ockwig, N. W.; Chae, H. K.; Eddaoudi, M.; Kim, J. *Nature* **2003**, *423*, 705−714. (b) Kitagawa, S.; Kitaura, R.; Noro, S. *Angew. Chem., Int. Ed.* **2004**, *43*, 2334−2375. (c) Ye, B.-H.; Tong, M.-L.; Chen, X.-M. *Coord. Chem. Rev.* **2005**, *249*, 545−565. (d) Férey, G. *Chem. Soc. Rev.* **2008**, *37*, 191−214. (e) Zhou, H.-C.; Long, J. R.; Yaghi, O. M. *Chem. Rev.* **2012**, *112*, 673−674. (f) Stock, N.; Biswas, S. *Chem. Rev.* **2012**, *112*, 933−969. (g) Cook, T. R.; Zheng, Y.; Stang, P. J. *Chem. Rev.* **2013**, *113*, 734−777.

(3) (a) Tranchemontagne, D. J.; Ni, Z.; O'Keeffe, M.; Yaghi, O. M. *Angew. Chem., Int. Ed.* **2008**, *47*, 5136−5147. (b) Park, J.; Sun, L.-B.; Chen, Y.-P.; Perry, Z.; Zhou, H.-C. *Angew. Chem., Int. Ed.* **2014**, *53*, 5842−5846. (c) Suzuki, K.; Takao, K.; Sato, S.; Fujita, M. *J. Am. Chem. Soc.* **2010**, *132*, 2544−2545.

(4) (a) Perry, J. J., IV; Perman, J. A.; Zaworotko, M. J. *Chem. Soc. Rev.* **2009**, *38*, 1400−1417. (b) Guillerm, V.; Kim, D.; Eubank, J. F.; Luebke, R.; Liu, X.; Adil, K.; Lah, M. S.; Eddaoudi, M. *Chem. Soc. Rev.* **2014**, *43*, 6141−6172. (c) Lee, E.; Kim, J.; Heo, J.; Whang, D.; Kim, K. *Angew. Chem., Int. Ed.* **2001**, *40*, 399−402. (d) Sudik, A. C.; Côté, A. P.; Wong-Foy, A. G.; O'Keeffe, M.; Yaghi, O. M. *Angew. Chem., Int. Ed.* **2006**, *45*, 2528−2533. (e) Park, J.; Hong, S.; Moon, D.; Park, M.; Lee, K.; Kang, S.; Zou, Y.; John, R. P.; Kim, G. H.; Lah, M. S. *Inorg. Chem.* **2007**, *46*, 10208−10213. (f) Nouar, F.; Eubank, J. F.; Bousquet, T.; Wojtas, L.; Zaworotko, M. J.; Eddaoudi, M. *J. Am. Chem. Soc.* **2008**, *130*, 1833−1835. (g) Zhang, Z.; Wojtas, L.; Zaworotko, M. J. *Chem. Sci.* **2014**, *5*, 927−931. (h) Meng, L.; Cheng, Q.; Kim, C.; Gao, W.-Y.; Wojtas, L.; Chen, Y.-S.; Zaworotko, M. J.; Zhang, X. P.; Ma, S. *Angew. Chem., Int. Ed.* **2012**, *51*, 10082−10085.

(5) (a) Liu, Y.; Kravtsov, V.; Walsh, R. D.; Poddar, P.; Srikanth, H.; Eddaoudi, M. *Chem. Commun.* **2004**, 2806−2807. (b) Sava, D. F.; Kravtsov, V. C.; Eckert, J.; Eubank, J. F.; Nouar, F.; Eddaoudi, M. *J. Am. Chem. Soc.* **2009**, *131*, 10394−10396. (c) Zhai, Q.-G.; Mao, C.; Zhao, X.; Lin, Q.; Bu, F.; Chen, X.; Bu, X.; Feng, P. *Angew. Chem., Int. Ed.* **2015**, *54*, 7886−7890. (d) Zou, R.-Q.; Jiang, L.; Senoh, H.; Takeichi, N.; Xu, Q. *Chem. Commun.* **2005**, 3526−3528. (e) Zou, R.-Q.; Sakurai, H.; Xu, Q. *Angew. Chem., Int. Ed.* **2006**, *45*, 2542−2546. (f) Cheng, A.-L.; Liu, N.; Zhang, J.-Y.; Gao, E.-Q. *Inorg. Chem.* **2007**, *46*, 1034−1035. (g) Xu, Q.; Zou, R.-Q.; Zhong, R.-Q.; Kachi-Terajima, C.; Takamizawa, S. *Cryst. Growth Des.* **2008**, *8*, 2458−2463. (h) Alkordi, M. H.; Brant, J. A.; Wojtas, L.; Kravtsov, V. C.; Cairns, A. J.; Eddaoudi, M. *J. Am. Chem. Soc.* **2009**, *131*, 17753−17755. (i) Zou, J.-Y.; Shi, W.; Zhang, J.-Y.; He, Y.-F.; Gao, H.-L.; Cui, J.-Z.; Cheng, P. *CrystEngComm* **2014**, *16*, 7133−7140.

(6) Orcajo, G.; Calleja, G.; Botas, J. A.; Wojtas, L.; Alkordi, M. H.; Sánchez-Sánchez, M. *Cryst. Growth Des.* **2014**, *14*, 739−746.

(7) (a) Fang, Q.-R.; Yuan, D.-Q.; Sculley, J.; Li, J.-R.; Han, Z.-B.; Zhou, H.-C. *Inorg. Chem.* **2010**, *49*, 11637−11642. (b) Tahmasebi, E.; Masoomi, M. Y.; Yamini, Y.; Morsali, A. *Inorg. Chem.* **2015**, *54*, 425−433. (c) He, J.; Yee, K.-K.; Xu, Z.; Zeller, M.; Hunter, A. D.; Chui, S. S.-Y.; Che, C.-M. *Chem. Mater.* **2011**, *23*, 2940−2947. (d) Hao, J.-N.; Yan, B. *Chem. Commun.* **2015**, *51*, 7737−7740.

DOI: 10.1021/acs.inorgchem.5b01659
Inorg. Chem. 2015, 54, 9678−9680